Astron. Astrophys. 359, 682–694 (2000)

ASTRONOMY
AND
ASTROPHYSICS

# Energy spectrum and chemical composition of cosmic rays between 0.3 and 10 PeV determined from the Cherenkov-light and charged-particle distributions in air showers

**The HEGRA-Collaboration**

**F. Arqueros[3], J.A. Barrio[2,3], K. Bernlöhr[1,⋆], H. Bojahr[6], I. Calle[3], J.L. Contreras[3], J. Cortina[3,2], T. Deckers[5], S. Denninghoff[2], V. Fonseca[3], J. Gebauer[2], J.C. González[3], V. Haustein[4,⋆⋆], G. Heinzelmann[4], H. Hohl[6], D. Horns[4], A. Ibarra[3], M. Kestel[2], O. Kirstein[5], H. Kornmayer[2], D. Kranich[2], H. Krawczynski[1,4], A. Lindner[4], E. Lorenz[2], N. Magnussen[6], H. Meyer[6], R. Mirzoyan[2], A. Moralejo[3], L. Padilla[3], D. Petry[2,6,⋆⋆⋆], R. Plaga[2], J. Prahl[4], G. Rauterberg[5], W. Rhode[6], A. Röhring[4], M. Samorski[5], D. Schmele[4], F. Schröder[6], W. Stamm[5], B. Wiebel-Sooth[6], M. Willmer[5], and W. Wittek[2]**

[1] Max-Planck-Institut für Kernphysik, Postfach 103980, 69029 Heidelberg, Germany
[2] Max-Planck-Institut für Physik, Föhringer Ring 6, 80805 München, Germany
[3] Universidad Complutense, Facultad de Ciencias Físicas, Ciudad Universitaria, 28040 Madrid, Spain
[4] Universität Hamburg, II. Institut für Experimentalphysik, Luruper Chaussee 149, 22761 Hamburg, Germany
[5] Universität Kiel, Institut für Experimentelle und Angewandte Physik, Leibnizstrasse 15, 24118 Kiel, Germany
[6] Universität Wuppertal, Fachbereich Physik, Gaussstrasse 20, 42097 Wuppertal, Germany

Received 6 April 1999 / Accepted 17 August 1999

**Abstract.** Measurements of the lateral distribution of Cherenkov photons with the wide-angle atmospheric Cherenkov light detector array AIROBICC and of the charged particle lateral distribution with the scintillator matrix of the HEGRA air-shower detector complex in air showers are reported. They are used in conjunction to determine the energy spectrum and coarse chemical composition of charged cosmic rays in the energy interval from 0.3 PeV to 10 PeV. With the atmospheric shower-front sampling technique these detectors measure the electromagnetic component of an extensive air shower via the lateral density distribution of the shower particles and of the Cherenkov photons. The data are compared with events generated with the CORSIKA program package with the QGSJET hadronic-event generator. Consistency checks performed with primary energy-reconstruction methods based on different shower observables indicate satisfactory agreement between these extensive air shower simulations and the experimental data. This permits to derive results concerning the energy spectrum and composition of charged cosmic rays.

The energy spectrum features a so called "knee" at an energy of $E_{\rm knee}$=$3.98^{+4.66}_{-0.83}(\rm stat) \pm 0.53(\rm syst)$ PeV. Power law fits to the differential energy spectrum yield indices of $-2.72^{+0.02}_{-0.03}(\rm stat) \pm 0.07(\rm syst)$ below and $-3.22^{+0.47}_{-0.59}(\rm stat) \pm 0.08(\rm syst)$ above the knee.

The best-fit elongation rate for the whole energy range is determined to 78.3 ± 1.0 (stat) ± 6.2 (syst) g/cm$^2$. At the highest energies it seems to decrease slightly. The best-fit fraction of light nuclei decreases from $37^{+28}_{-21}$% (combined statistical and systematic) to $8^{+32}_{-8}$% (combined statistical and systematic) in the energy range discussed here. A detailed study of the systematic errors reveals that a non-changing composition cannot be excluded.

**Key words:** ISM: cosmic rays

## 1. Introduction

The origin of extra solar cosmic rays (CR) is one of the important unresolved astrophysical questions. Galactic shell type supernova remnants (SNR) have been proposed as plausible acceleration sites for cosmic rays up to energies of several PeV (Völk 1997) and - for very massive SN progenitors - to even higher energies (Biermann et al. 1995). Recently direct experimental evidence for electron acceleration in these objects has been found in the X-ray (Koyama et al. 1995; Koyama et al. 1997; Allen et al. 1997) and TeV $\gamma$-ray range (Tanimori et al. 1998). Somewhat surprisingly, similar searches for evidence of hadron acceleration have only yielded upper limits on the expected $\gamma$-ray emission from the interaction of the hadrons with interstellar matter up to now (Prosch et al. 1996; Heß 1997; Buckley et al. 1998).

An indirect approach to distinguish between different theoretical models aiming to describe the acceleration of charged

*Send offprint requests to*: R. Plaga (plaga@mppmu.mpg.de)
⋆ Now at Forschungszentrum Karlsruhe, P.O. Box 3640, 76021 Karlsruhe, Germany
⋆⋆ Now at Line Consulting AG, Hamburg
⋆⋆⋆ Now at Universidad Autónoma de Barcelona, Institut de Física d'Altes Energies, 08193 Bellaterra, Spain

cosmic rays (CR) is to measure the energy spectrum and composition of CR and compare the results with model predictions. Here the energy regime around the so called "knee" between 1 and 10 PeV is especially interesting(Watson 1997). In this energy range the all-particle CR energy spectral slope - that is constant within measurement errors for lower energies - suddenly increases. The riddle of the origin of the knee and of the cosmic radiation with energies exceeding it, is not yet finally resolved. The following general solutions have been discussed:

1. The change in index is due to some propagation effect in an "original" cosmic-ray population that displays an unbroken power law from low energies up to energies above the knee. The most popular idea is that the energy dependence of the diffusion constant of cosmic rays in the Galaxy could change in the knee region (Peters 1961; Ptuskin et al. 1993). Because of the dependence of the diffusion constant on the nuclear charge Z a modest decrease in the fraction of "light" elements (hydrogen and helium) would be expected. In the simplified chemical model we use below (heavy elements modelled by 65 % oxygen and 35 % iron, light elements by 40 % hydrogen and 60 % helium) the fraction of light elements would be expected to decrease from an assumed value of 60% below the knee to 43% above the knee. In such a model (barring a special cancellation of effects) the knee is expected to be a relatively smooth feature, extending over about a decade in energy. A principal problem with this approach is that no plausible Galactic source of cosmic rays has been identified which is quantitatively capable of producing the "original" cosmic-ray population.
2. The knee signals in some way the maximum energy for the sources responsible for low energy cosmic rays. The cosmic rays at higher energies could be "re-accelerated" low energy cosmic-rays, e.g. at the shock front of a Galactic wind (Jokipii & Morfill 1987) or an ensemble of shock fronts in clusters of massive stars (Bykov & Toptygin 1997). In this case a phenomenology similar to the diffusion model in the previous paragraph would be expected. Alternatively, above the knee a completely new population of cosmic rays dominates. In this case typically dramatic changes in chemical composition are expected, e.g. to pure hydrogen in the extragalactical model of Protheroe & Szabo (1992) and nearly pure heavy elements (fraction of light elements $<$ 0.3 far above the knee) in a model with special SNRs by Stanev et al. (1993). The special properties of these new sources could in principle allow to understand a knee relatively "sharp" in energy.

To definitely discriminate between a composition changing as expected in models with an energy dependent diffusion constant (discussed above under 1.) and an unchanging composition, it is necessary to achieve an error of smaller than $\pm$ 10 % in the experimental determination of the fraction of light elements in the total cosmic radiation above the knee.

While the cosmic-ray composition and energy spectrum are well known from direct balloon and space-borne observations up to energies of about 100 TeV, no general agreement has been reached at higher energies (Watson 1997). The results obtained for CR around the "knee" suffer seriously from the fact that due to the low flux of CR above 1 PeV, only large ground based installations observing the extensive air showers (EAS) induced by cosmic rays in the atmosphere can provide experimental data. However the sensitivity of EAS observables to the mass of the primary CR is weak. The analyses are rendered even more difficult due to theoretical uncertainties concerning the high energy interactions in the atmosphere (Knapp et al. 1996; Gaisser 1997).

Here we present an analysis of EAS between 300 TeV and 10 PeV which restricts to observables related to the electromagnetic shower component. In the following sections the experimental setup (Sect. 2), the Monte-Carlo simulations (Sect. 3), the event reconstruction (Sect. 4) and analysis methods (Sect. 5) are described. Sect. 6 presents the results concerning the CR energy spectrum and the coarse mass composition. A more detailed study of the systematic errors and a discussion of methods to analyse the composition without relying on the absolute penetration depth are discussed in Sect. 7. The paper ends with conclusions in Sect. 8.

## 2. The experimental setup

The air-shower detector complex HEGRA covers an area of $180{\cdot}180\,\mathrm{m}^2$ at a height of 2200 m a.s.l. (790 g/cm$^2$) (Lindner 1997; Karle et al. 1995; Krawczynski et al. 1996; Rhode et al. 1996). In the present analysis only data of the scintillator array and part of the AIROBICC array were used. The former consists of 243 huts with plastic scintillators of an area of 0.96 m$^2$, covered with 5 mm of lead on a grid with 15 m spacing (with a denser part with 10 m spacing in the centre of the array). The part of the latter used in this analysis is formed by 49 open photo-multipliers fitted with Winston cones, restricting the viewed solid angle to 0.835 sr and measuring the air Cherenkov light of EAS on a grid with 30 m spacing. The gain nonlinearity of all components in the Cherenkov-light measurement was carefully checked, both with a LED light source with variable light intensity and a direct charge source. While the used Cherenkov light photomultiplier tubes were found to be linear, the used amplifier showed an antilinearity (gain rises with input amplitude) which was corrected in the data analysis. Above 10 PeV the amplifier begin to show signs of saturation and therefore no data above 10 PeV are included in the present analysis. The trigger conditions used for the data analysed here demand a signal from at least 14 scintillator or 6 AIROBICC stations within 150 ns. This corresponds to an energy threshold for primary protons and iron nuclei of 25 and 80 TeV respectively.

## 3. Monte Carlo simulations

EAS events were simulated using the CORSIKA code in its versions 5.20 with the QGSJET/GHEISHA options (Knapp & Heck 1993; Heck et al. 1998)). This generator is based on the quark-gluon string model (QGS) with an allowance for semihard processes (JET) (Kalmykov et al. 1997). Complex nuclei were treated with the "complete fragmentation" ansatz. The energy cutoff for particles of the electromagnetic cascade

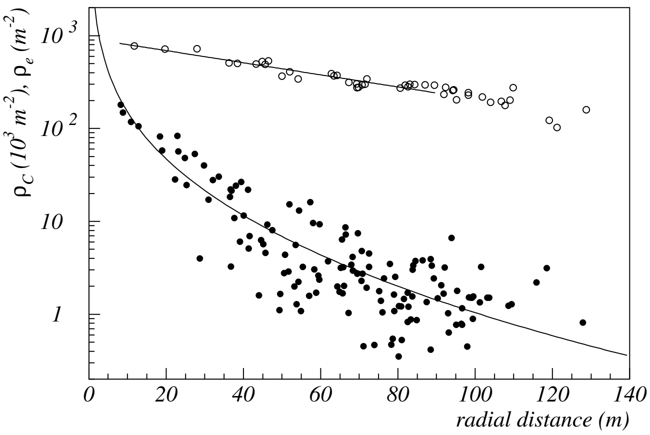


**Fig. 1.** The Cherenkov-light ($\rho_C$, open circles, in $10^3\times$ photons/m$^2$) and the actually measured (under lead coverage, see text) charged-particle density ($\rho_e$, full circles, in 1/m$^2$) as determined in a single observed shower. Each open (closed) circle corresponds to the light (charged particle) density determined by one AIROBICC (scintillator) station. The NKG function has been fitted to the charged-particle distribution and an exponential function to the Cherenkov light distribution in a 7.5–90 m radial interval (full lines). The energy of this event was 2.1 (2.8) PeV if induced by a proton (iron) nucleus.

was set to 3 MeV. Proton, helium, oxygen and iron induced showers were produced at zenith angles of 0°,6°, 12° and 18° at discrete energies between 300 TeV and 10 PeV (4400 independent showers of which 1000 are above 1 PeV) as well as an independent sample with a continuous energy distribution at zenith angles of 6° and 12° between 50 TeV and 1 PeV (4330 independent showers) and following a power law of $E^{-1}$ between 2.5 PeV and 6.5 PeV (240 showers). The events continuously distributed in energy were spectrally weighted and used in the fits to infer the chemical composition (Sect. 5.2), while the samples with discrete energies were employed to develop the reconstruction methods and to correct the results obtained with biased estimators of the primary energy (Sect. 5.1). Note that the simulation of an EAS induced by a 1 PeV primary proton including the Cherenkov light production requires about 3 h CPU time on a 300 MHz Pentium-II PC (during the same time the HEGRA experiment registers more than 350 showers with energies larger than 1 PeV).

The detector performance was modelled with two independent detector simulations: a full detector simulation (Martinez et al. 1995), and an empirical simulation using measured response functions (Haustein 1996; Horns 1997). Each independent generated EAS was used 20 times with core positions inside and outside the HEGRA area to take into account the detector related fluctuations of observables and to check the event selection criteria. With the standard cuts described below, each shower was used on the average two times in the discrete and once in the continuous MC sample.

Special care has been taken to simulate the density profile and absorption features of the atmosphere above La Palma correctly. Weather balloon measurements as well as comparisons between TeV photon data registered by the HEGRA system of imaging air Cherenkov telescopes and simulations were employed for this purpose (Bernlöhr 1999; Konopelko et al. 1999). The shower development and light emission were modelled with the U.S. standard atmosphere, and the light propagation was then simulated with a special program able (Haustein 1996), assuming a tropical maritime atmosphere for the summer. This atmosphere is a good approximation for the conditions at Tenerife, an island neighbouring the experimental site (Bernlöhr 1999).

## 4. Event reconstruction and data selection

The core position of an EAS is reconstructed independently from the data of the scintillator matrix and from AIROBICC where the latter data allow to tag core positions beyond the HEGRA boundary. If the core position lies inside the area covered with detector elements the scintillator derived core coordinates have a resolution of $\sigma(\mathrm{core}) = 2(5)\,\mathrm{m}$ for protons (iron) at energies above 300 TeV (a little more accurate compared to AIROBICC mainly due to the smaller grid distances of the scintillator huts). The direction of the primary particle is reconstructed nearly independently from the scintillator and AIROBICC arrival time data (where the scintillator derived core position is used here).

The particle density measured by the scintillator array is fitted by the NKG formula (Greisen 1956) with a Moliére radius of 106 m, yielding the shower size $N_s$ and an *age* value. $N_s$ is a factor ≈1.6 larger than $N_e$ (the "true" shower size at detector level, denoting the number of charged particles above a kinetic energy of 3 MeV) due to coverage of the detector huts with a lead layer and the fact that the NKG function does not correctly parametrise the electromagnetic part of hadronic showers.

The dependence of the Cherenkov photon density $\rho_\mathrm{c}$, as measured by AIROBICC, on the distance r from the shower axis can be well described by an exponential in the region 20 m < r < 100 m (Patterson & Hillas 1983):

$$\rho_\mathrm{c}(\mathrm{r}) \;=\; \mathrm{a}\cdot\exp(\mathrm{r}\cdot \mathit{slope}). \qquad (1)$$

The parameter *slope* (in units of [1/m]) is the most important one in our analysis methods. As an illustration Fig. 1 shows the lateral charged-particle and Cherenkov-light distributions for a single shower.

The amplitude calibration of the scintillator array is done for samples of 50000 events by comparing the ADC spectra of the individual huts - which display a single peak essentially corresponding to the energy deposited by minimum ionising electrons and muons - with the result of MC simulations for identical conditions. The absolute amount of the air Cherenkov light registered by AIROBICC was calibrated by comparing the energy inferred from the lateral Cherenkov light density in the spectral range from 300 nm to 500 nm registered at a shower core distance of 90 m (referred to as $L_{90}$ in the following) and the energy derived from $N_s$ and *slope* in the interval $2.5 < \log_{10}(E(N_s, \mathit{slope})/\mathrm{TeV}) < 2.75$ (refer to Sect. 5.1 below for energy reconstruction methods). The absolute Cherenkov-light calibration thus depends on the CR mass composition, because we do not apply a primary-mass independent energy reconstruction here. We used the low-energy composition at 100 TeV as specified by Wiebel-Sooth et al.(1998) (60 % light elements, see below Sect. 5.2 for details) for this calibration. If a pure proton (iron) composition is assumed the energy reconstructed from Cherenkov light alone is shifted by 3 (13)% to higher (lower) energies.

To select well-reconstructed events the EAS core positions and directions as reconstructed with AIROBICC and the scintillator matrix are demanded to be consistent. Additional cuts ensure the quality of the directional as well as the fits to the lateral particle and Cherenkov light density distributions. Events with the true shower-core position within the HEGRA array boundaries for the detector components used in this analysis (distance to edge of array $> 10$ m) and a zenith angle below $15^0$ are used for the further analysis. The efficiency to select EAS events with true core positions in the regarded $160{\cdot}160\,\mathrm{m}^2$ area is about 98% for primary energies above 300 TeV (independent of the primary mass). The contamination of the sample with EAS, where the true shower cores lay beyond the HEGRA boundary but which were erroneously reconstructed to fulfil the cuts is less than 1% from our simulations.

Nights with perfect weather conditions are selected by data of the Carlsberg Meridian Cycle (B.Argyle, priv.comm.) and by comparing the Cherenkov light measurements with data from the scintillators for samples of 50000 events (accumulated in about one hour with the used setup and trigger conditions). The data set solely contains nights without any technical problems of the used detector stations. In total it comprises (dead-time corrected) an on-time of 208 h. This corresponds to about 150000 events after all cuts with an energy above about 100 TeV and a zenith angle below $15^0$.

## 5. The analysis methods

Monte Carlo simulations revealed that the distance $\mathrm{d_{max}}$ between detector and shower maximum (defined as the point in the shower development with the maximal number of charged particles) can be reconstructed independently of the primary mass with the shape parameter *slope* of the lateral Cherenkov light density distribution:

$$\mathrm{d_{max}} = [680 + slope \cdot 20880\,\mathrm{m}]\,\mathrm{g/cm^2}. \quad (2)$$

From this relation the distance to the shower maximum is determined with a resolution (i.e. root mean square (RMS) of a $\mathrm{d_{max}}$(true)-$\mathrm{d_{max}}$(reconstructed) distribution) ranging from 40 g/cm$^2$ at 300 TeV to 20 g/cm$^2$ at 10 PeV (including all detector effects but no systematic error in the mean $\mathrm{d_{max}}$). The most important technical improvement in the data presented here to previous experiments is that these values are distinctly smaller than the width of natural shower fluctuations of proton induced showers in the atmosphere (see below Table 3). This makes the shape of the penetration-depth distribution a sensitive parameter for the chemical composition (see Sect. 7). Simple geometrical relations permit to infer $X_{\mathrm{max}}$, the depth of the shower maximum in the atmosphere, from $d_{\mathrm{max}}$. Relation 2 is only weakly energy dependent (Lindner 1998a). This dependence is neglected here.

### 5.1. Energy reconstruction

Methods have been developed to reconstruct the primary CR energy from the scintillator and AIROBICC data *independently* of the primary mass with an accuracy better than 35% (Lindner 1998a; Cortina et al. 1997a; Cortina 1998). However, these methods lead to a relatively strong correlation between reconstructed energy and $X_{\mathrm{max}}$ (showers with a maximum position that fluctuated to smaller values compared to the mean $X_{\mathrm{max}}$, are reconstructed with higher energies). In order to infer the chemical composition, a careful modelation of the response function between the variables $N_s$ (or $L_{90}$) and *slope* on the one hand and energy and composition (or penetration depth) on the other hand (e.g. via two-dimensional regularised unfolding) is then necessary. Such procedures have been employed in some analyses of HEGRA data (Wiebel-Sooth 1998; Kornmayer 1999). Two reasons lead us to prefer to circumvent the mentioned problem with the use of two simpler energy estimators here.

One reason is that the methods described below are based on physically transparent properties of air-showers inferred from the Monte-Carlo simulations. Whether these properties really hold, is tested to some degree using different energy estimators with different biases and comparing the obtained results. These consistency checks are an important advantage over more refined and complete methods when it is doubtful how well the Monte-Carlo simulation describes the data. The other reason is that the Monte Carlo statistics at the highest energy is still rather limited and mean shower properties are inferred with higher certainty than a complete response matrix. The mass independent energy reconstruction methods will be applied to the data in a forthcoming publication together with a discussion of the influence of different EAS simulations. The energy estimators used in this paper and described below are based on $N_{\mathrm{s}}$ and *slope*, or $L_{90}$. Both estimators are used under the assumption that all primary CR are either protons or iron nuclei. These extreme assumptions lead to a bias which then has to be corrected for.

Using $N_{\mathrm{s}}$ and *slope* the energy of the primary cosmic-ray nucleus is reconstructed in two basic steps here (Lindner 1998b; Cortina et al. 1997a; Plaga et al. 1995): first *slope* (a measure of the distance to the shower maximum) is combined with $N_{\mathrm{s}}$ to estimate the number of particles in the shower maximum which is proportional to the energy contained in the electromagnetic component of the EAS. In the second step a specific primary mass is assumed; with the assumption of primary proton (iron) we denote the methods as 1 (2). This allows to calculate the primary energy from the energy deposited in the electromagnetic component. The following relation was used in our analysis:

$$log(E[\mathrm{TeV}]) = a \cdot log(N_s(\mathrm{max})) + b. \quad (3)$$

Here $a, b$ were obtained from the discrete Monte Carlo data as 0.965, $-2.545$ (0.890, $-2.010$) for protons (iron). $N_{\mathrm{s}}(\mathrm{max})$ is

**Table 1.** Summary of the energy reconstruction methods 1–4 as discussed in the text.

| Method # | parameter used | primaries assumed to be |
|---|---|---|
| 1 | $N_{\rm s}$ and *slope* | protons |
| 2 | $N_{\rm s}$ and *slope* | iron nuclei |
| 3 | light density $L_{90}$ | protons |
| 4 | light density $L_{90}$ | iron nuclei |

the shower size at the maximum of shower development and is inferred from $N_s$ as:

$$N_{\rm s}(\max)/N_{\rm s} = a_0 + a_1 slope + a_2 slope^2 + a_3 slope^3 \qquad (4)$$

with $a_n$ given as (0.57833, −85.146, 6181.8, −714054) for all primary nuclei. This procedure is valid because the shape of the shower development is only weakly dependent on the mass of the CR nucleus A, especially after the shower maximum (Lindner 1998a). Only the fraction of the total energy fed into the electromagnetic cascade depends on A for a given energy per nucleus. The comparison of the results assuming initially proton and iron primaries is a consistency check for the dependence of shower size at the maximum of shower development on the energy per nucleon.

Alternatively the energy is reconstructed from the AIROBICC data alone (method 3 (4) with the assumption of proton (iron) primaries). Here it turns out that $L_{90}$ is a good estimator of the energy contained in the electromagnetic EAS cascades. From simulations the relation

$$log(E[\text{TeV}]) = a \cdot log(L_{90}[\text{photons/m}^2]) + b \qquad (5)$$

was derived, where the coefficients $a$ and $b$ are given as $0.958, -1.810$ $(0.840, -1.061)$ for primary protons (iron). *slope* (the parameter used to estimate the primary mass composition, see next Sect.) is not involved in this energy reconstruction. For ease of reference the four energy-reconstruction methods are summarised in Table 1. The agreement of analyses based on $N_s$ and $L_{90}$ is a consistency test for the accurate description of the longitudinal shower development by the Monte Carlo simulation.

Naturally (because the fraction of the primary energy deposited in electromagnetic cascades depends on the energy per nucleon of the primary particle) the mean of the calculated energy is only correct for the assumed particle type (Fig. 2). The biases shown in Fig. 2 have to be corrected for, to derive the real energy spectrum and CR mass composition from our measurements (see Sect. 5.2, 5.3). In order to check that our final results do not depend on the assumed primary-particle mass, we shall always compare the results based on the four energy reconstruction methods below.

The distribution of the reconstructed energy compared to the simulated energy is shown for examples in Fig. 3. Note that the energy reconstruction from $L_{90}$ alone shows Gaussian distributions while the energy obtained from $N_s$ and *slope* exhibits tails to high values which have to be taken into account properly in the analyses. Fig. 4 shows the relative energy resolution achieved for different primary particles and energy reconstruction methods 1 and 3. If $N_s$ is involved in the energy reconstruction the energy resolution is limited by the experimental accuracy of the shower size determination at the detector level. Due to the smaller $N_s$ of iron compared to proton induced EAS the accuracy of the energy reconstruction for iron showers is a little worse than for proton showers. The energy resolution

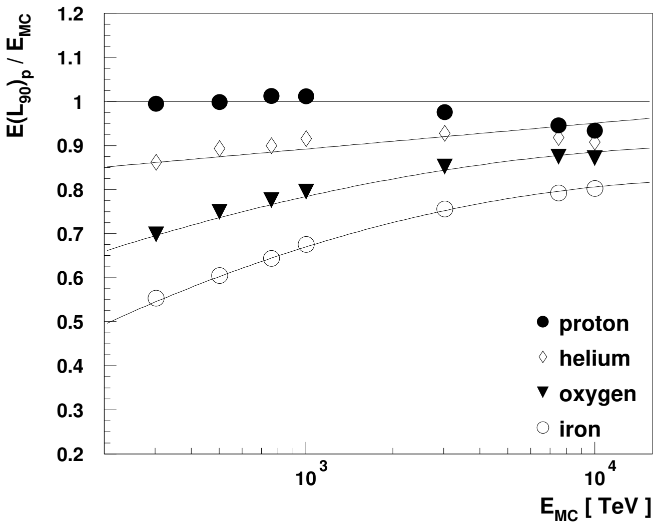


**Fig. 2.** The bias of the energy reconstruction as a function of primary energy for different primary masses. Shown is the ratio of the reconstructed energy with method 3, divided by the true energy (from the Monte-Carlo simulation). Very similar results are obtained from $N_s$ and *slope*. The lines show fits used for convolution procedures to determine the final results (see text).

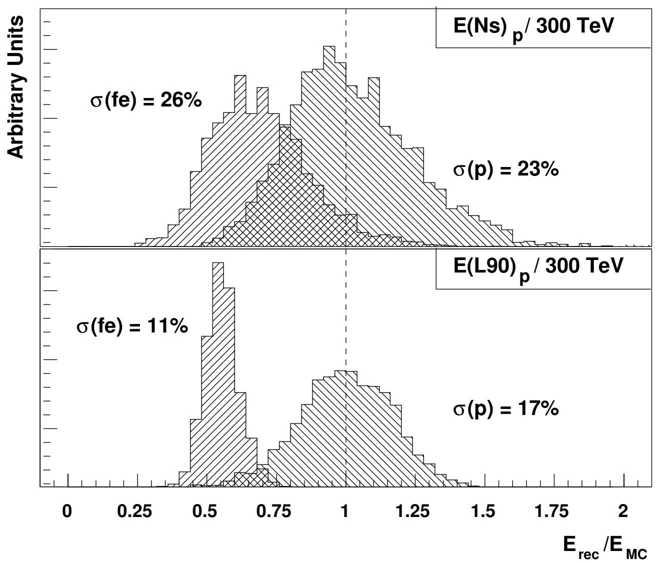


**Fig. 3.** Distribution of the ratio of reconstructed to MC generated energy (300 TeV) for two primaries (left distribution: iron nuclei, right distribution: protons) and the two different energy reconstruction methods discussed in the text. Each distribution is normalised to the same area.

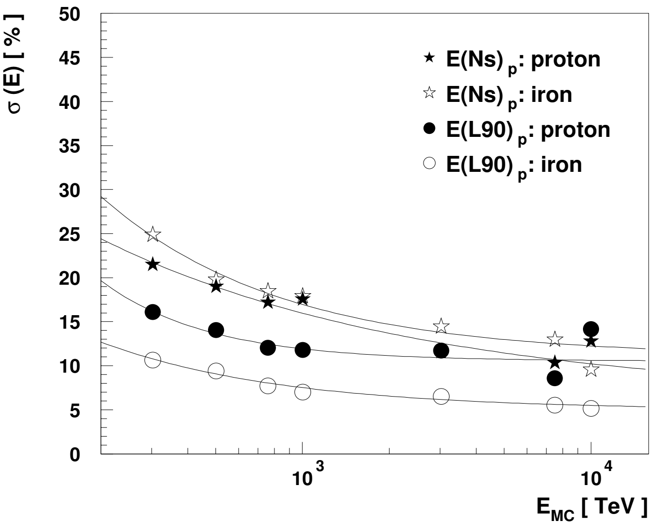


**Fig. 4.** The energy resolution obtained for different primary nuclei as a function of the generated MC energy. $N_s$ in brackets denotes an energy reconstruction that combines the measured shower size at detector level and *slope*, $L_{90}$ denotes the results obtained from the Cherenkov light density alone. The energy reconstruction was always performed assuming that the primaries are protons (referred to as methods 1 (stars in the figure) and 3 (dots in the figure) in the text; this fact is symbolised by the subscript "p" on the energy). The "proton" (filled symbols) "iron" (open symbols) after the colon indicate the primary for which the energy resolution was determined. The lines show fits used for convolution procedures to determine the final results (see text).

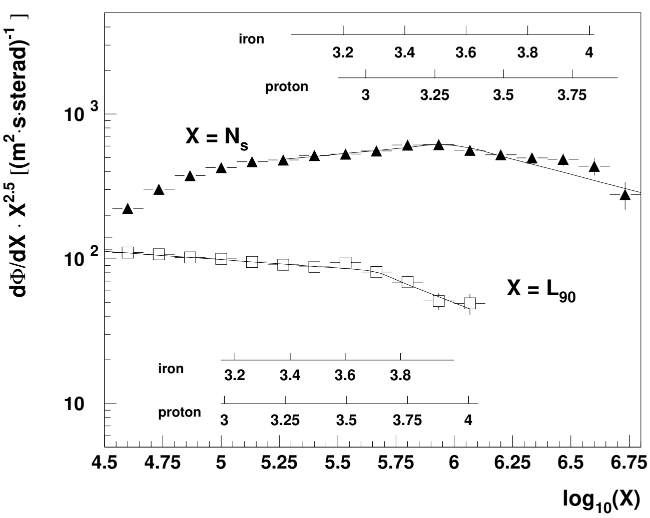


**Fig. 5.** The differential shower-size spectrum and "light-density at 90 m core distance ($L_{90}$)" spectrum. The values used for the construction of these spectra, were employed for the energy reconstruction. The full lines indicate the best fit in the range 5.3–6.8 and 4.5–6.1 for $N_s$ and $L_{90}$ respectively. Two power laws which meet in a single flux value ("the knee") were assumed. The best-fit power law indices are (-2.35/-2.92) and (-2.61/-3.13) (before/after) the knee at a position of $\log_{10}(N_s)$/$\log_{10}(L_{90})$ = 5.99/5.64 for the shower size/light density respectively. The energy scales were derived under the assumption that the primaries are all protons, resp. iron nuclei for shower size (upper scales) and light density (lower scales).

obtained from $L_{90}$ is mainly determined by fluctuations in the shower development (being larger for proton than iron induced showers) and could not be decreased much by improving the detector.

In all analyses below we bin the data in six equidistant energy intervals from $\log_{10}E_{\rm reconstructed}$ [TeV]=2.5 to $\log_{10}E_{\rm reconstructed}$ [TeV]=4.0 (see e.g. Fig. 9). Event samples defined to contain events in a certain reconstructed-energy interval for the four energy-reconstruction methods then contain events with different true primary energies. It should always be kept in mind that these four samples are not independent because they are all based on the same total data sample.

### *5.2. Chemical composition*

The composition of CR is determined by analysing the EAS penetration depth ($X_{\rm max}$) distributions in intervals of the reconstructed primary energy. Information is contained in the differences of the mean $X_{\rm max}$ values for different primaries (protons penetrate about 100–130 g/cm$^2$ deeper than iron in the energy range considered here) and also in the the different fluctuations of the shower maxima position. Including experimental resolution we obtained RMS$(X_{\rm max}, p) \;=\; 90\,{\rm g/cm}^2$ and RMS$(X_{\rm max}, Fe) \;=\; 50\,{\rm g/cm}^2$ at 1 PeV). The RMS values of the depth distributions of Monte-Carlo events slightly decrease with rising energy, an effect that is partly due to an improving measurement of *slope*.

We perform an analysis which uses both of these parameters in one fitting procedure. As the error from such an analysis turns out to be already quite large, we do not perform an analysis based on mean penetration depth alone. An analysis based mainly on the fluctuation of penetration depths is discussed in Sect. 7.

The present data are not sensitive enough on the chemical composition to allow a analysis with several mass groups; therefore we restrict ourselves to a determination of the fraction of light nuclei (protons and helium) by fitting the expected to the measured $X_{\rm max}$ distributions. To define the MC expectations for light nuclei, the generated distributions for primary protons and helium nuclei are added with weights of 40% and 60% (the ratio derived from direct measurements at energies around 100 TeV (Wiebel-Sooth et al. 1998)). The distribution of heavier nuclei is constructed analogously by summing 65% oxygen and 35% iron induced EAS. Variations in this ratio at higher energies are possible and are an additional potential source for systematic errors that is not further considered below.

The spectrally weighted Monte-Carlo data are fitted to the measured penetration-depth distributions for each of the four energy-reconstruction methods. Because spectrally weighted Monte-Carlo data were available only for the energy bins $\log_{10}$ $(E_{\rm reconstructed})$ = 2.5–2.75 and 3.5–3.75 the energy bins between 2.5–3.25 (3.25–4) were fitted with the former (latter) distribution. The MC events used in energy intervals other than the two for which the simulations were done, were shifted in the mean penetration depth according to the elongation rate of the various elements. To avoid any systematic uncertainties related to imperfect parameterisations of the MC distributions and to take into account the statistical uncertainty of the simulated event sample we directly fit the MC generated distributions to the experimental data.

Due to the primary dependent energy-reconstruction method the results for the "fraction of light nuclei" (abbreviated "(p + $\alpha$)/all" below) are biased. The results for these fits in the chosen energy bins are shown for method 3 in Fig. 9. The obtained (p + $\alpha$)/all ratios are then corrected for the A dependent bias which is illustrated in Fig. 2. The correction can be described as a single overall factor for the (p + $\alpha$)/all ratio for each energy bin - rather than a transformation of the penetration depth distribution - to a good approximation because of the independence of our energy reconstruction methods of $X_{\max}$ as discussed in Sect. 5.1. These correction factors were derived from spectrally weighted Monte-Carlo data via determining the true (p + $\alpha$)/all in the Monte Carlo that yields the fitted biased (p + $\alpha$)/all in the given reconstructed-energy bin. In this way the ratio of biased to true (p + $\alpha$)/all at the true mean energy of the Monte-Carlo showers in the energy bin for a given energy reconstruction method is obtained. As an illustration the correction factors for the case of energy reconstruction method 3 are shown in Table 2.

For the spectral weighing of the Monte-Carlo sampling a primary-spectrum as obtained from low-energy measurements (Wiebel-Sooth et al. 1998) with a power law index of $\alpha$=$-2.67$ and a "knee" at 3.4 PeV with a change in the power-law index to $\alpha$=$-3.1$ was assumed. An iterative repetition of this procedure with the energy spectrum as inferred below from the present data is possible. However, it was found that the contribution to the systematic error introduced by not performing the iterations is negligible for the initial parameters chosen.

Two Monte-Carlo samples were used for bias corrections in this work, the Monte-Carlo sample with events continuously distributed in energy, mentioned in Sect. 3, and a "toy Monte-Carlo sample" with unlimited statistics, which was created by randomly choosing all measured parameters (like reconstructed energy, $X_{\max}$ etc.) of a shower with a given true primary energy from one dimensional distributions inferred from the Monte Carlo sample with discrete energies. It was checked that the corrections obtained with these samples are very similar in energy regions where the continuously distributed Monte-Carlo data were available.

### *5.3. Energy spectra, elongation diagrams and penetration depth fluctuations*

Energy spectra obtained with the four energy-reconstruction methods were corrected for the A dependent bias by dividing the flux values in bins with true and reconstructed energy in the Monte-Carlo samples. The chemical composition as determined with the methods in the previous Sect. is used. These factors were applied to the flux in each energy bin when going from reconstructed (Fig. 6) to true energy (Fig. 7).

$X_{\max}$ as a function of true energy is obtained if the mean $X_{\max}$ is plotted at the mean true energy of the events in a given reconstructed-energy bin, as calculated with the measured chemical composition. This procedure leads to correct results as long as the elongation rate of different nuclei is identical; this is fulfilled to a good approximation for all hadron generators.

**Table 2.** The fraction of light elements (uncorrected) and correction factor for the A dependent bias with energy reconstruction method 3. The uncorrected ratio has to be multiplied by this factor to yield the unbiased ratio. The energy intervals are specified as the logarithm to the base of ten in units of TeV.

| Reconstructed energy | p + $\alpha$/all | correction factor |
|---|---|---|
| 2.5–2.75 | 0.502 | 0.741 |
| 2.75–3. | 0.493 | 0.763 |
| 3.0–3.25 | 0.553 | 0.813 |
| 3.25–3.5 | 0.406 | 0.800 |
| 3.5–3.75 | 0.272 | 0.806 |
| 3.75–4. | 0.09 | 0.820 |

The RMS of the shower penetration depth distributions were directly calculated from the distributions calculated with a given energy-reconstruction method, i.e. no procedure to remove the bias was applied. These results were compared with RMS values from Monte Carlo data treated in the same way.

### *5.4. Experimental statistical and systematic uncertainties*

For the energy spectrum the statistical uncertainties correspond to the square root of the energy-bin contents N for the energy spectrum and the mean $X_{\max}$ divided by $\sqrt{N}$ for the penetration depth. In all other cases statistical errors were obtained by changing the fit parameter from its best-fit value until the $\chi^2_{\rm red}$ increases by 1. In case of best fit $\chi^2_{\rm red}$'s in excess of 1.5 the best fit value of the fit parameter was increased until $\chi^2_{\rm red}$ doubled.

Systematic uncertainties of the Monte-Carlo simulation of hadronic air-showers - estimated by using different hadronic Monte-Carlo generators - will be considered in a forthcoming paper. Here we concentrate on experimental uncertainties related to the *slope* reconstruction. These are contributions from remaining uncertainties in the characteristics of the AIROBICC amplifier (3% uncertainty for *slope*) and non-perfect knowledge of the layer structure and the light absorption of the atmosphere above the detector (4% and 2%). Models of the atmosphere have been carefully checked using the large statistics of photon induced air showers which were registered with the HEGRA imaging air Cherenkov telescopes in 1997 (Konopelko et al. 1999). Added in quadrature the systematic uncertainty of *slope* amounts to 5%. The mean $X_{\max}$ for 300 TeV proton (iron) induced showers is then determined with an uncertainty in the absolute values of 20 (13) g/cm$^2$. The uncertainties for different primaries are strongly correlated.

For the chemical composition, the energy spectrum and the variation of $X_{\max}$ with energy (elongation rate), the systematic error was evaluated by changing all *slopes* by 5% (the systematic error of this parameter) up or down. The whole analysis, including energy reconstruction, was then repeated and the deviation of the results thus obtained to the original ones was

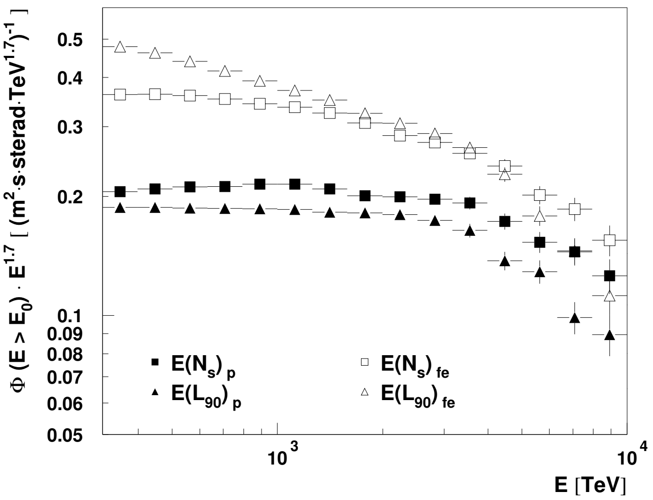


**Fig. 6.** The integral energy spectra obtained with the four energy reconstruction methods denoted with different symbols. Filled square: Method 1, open square: method 2, filled triangle: method 3, open triangle: method 4. The biases of the energy reconstruction have not been corrected for.

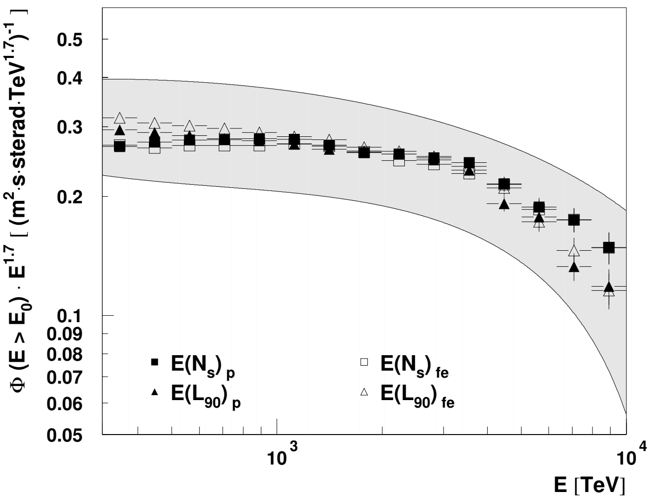


**Fig. 7.** Integral cosmic-ray spectrum corrected for the A dependent bias. The shaded area denotes the systematic error. Symbols are the same as in the previous figure.

taken as the systematic error (errors beyond the tick mark in Figs. 10,11 and shaded bands in Figs. 7,8). The shaded band in Fig. 11 is obtained by varying the best-fit composition within its total systematic and statistical error. In the case of the elongation rate the systematic error was found to be dominated by the differences in the four energy-reconstruction methods, this is dicussed in detail in the Results Sect. 6.4. In case of the RMS of the penetration depths, the spectral fit parameters (knee position, power-law indices) and the elongation rate, the systematic error was estimated as the sample standard deviation of the best fit parameters obtained with the four energy-reconstruction methods.

## 6. Results

In this Sect. the methods explained in Sect. 5 are applied to the data set discussed in Sect. 4.

### 6.1. $N_{\rm s}$ and $L_{90}$ spectra

Fig. 5 shows the $N_{\rm s}$ and $L_{90}$ spectra. These spectra display a relatively sharp knee at values consistent with a primary energy for the knee as determined below.

### 6.2. Energy spectra

Fig. 6 displays the integral energy spectra uncorrected for an A dependent bias obtained with the four reconstruction methods. The differences in absolute normalisation and spectral slope originate from the different mass dependent biases. After the correction of the chemical bias the integral spectra are similar (Fig. 7). This nontrivial fact is in favour of the internal consistency of data analysed here; a longitudinal shower development different from the one predicted by the Monte Carlo or errors in the calibration of $L_{90}$ and $N_s$ could have spoiled the agreement of spectra obtained with different energy reconstructions. The differential energy spectrum is shown in Fig. 8. A steepening of the energy spectrum is visible around an energy of 4 PeV. There seems to be no "fine structure" in the energy spectrum around the knee in excess of 20 %. Apparent structure with smaller amplitudes that appears in the spectrum reconstructed with a given energy-reconstruction method is not reproduced with other methods. This is expected due to the A dependent bias of our energy-reconstruction methods (see Fig. 2). Note that with these methods, a potential structure in the energy spectrum consisting of different nuclei is smeared out. If two different power laws, smoothly connected at the knee (corresponding to a "sharp" knee), are fitted to the differential spectra we obtain:

– a "knee" position of $E(\mathrm{Knee}) = 3.98^{+4.66}_{-0.83}(\mathrm{stat}) \pm 0.53(\mathrm{syst})$ PeV,
– a spectral index of $-2.72^{+0.02}_{-0.03}(\mathrm{stat}) \pm 0.07(\mathrm{syst})$ below and $-3.22^{+0.47}_{-0.59}(\mathrm{stat}) \pm 0.08(\mathrm{syst})$ above the knee.

The reduced $\chi^2$ values of the fits to the differential spectrum (12 d.o.f.) were 6.75, 4.03, 3.53 and 1.47 with energy reconstruction methods 1 to 4 respectively. Some of these values are much larger than one. It is then difficult to specify a statistical error; we specify the statistical errors for method 4 that has a marginally acceptable reduced $\chi^2$ value. The large $\chi^2$ values for the analysis with energy-reconstruction methods 1–3 can be interpreted as an argument in favour of a knee not absolutely sharp in energy. However, the fact that one of the fits is acceptable on the 90 % confidence level means that we cannot reject the hypothesis of a "sharp" knee (two power laws with no transition region) within our systematic errors. The large statistical error on the knee position further indicates that we cannot reject the hypothesis of a spectrum without a knee in the limited energy range of this analysis with high significance.

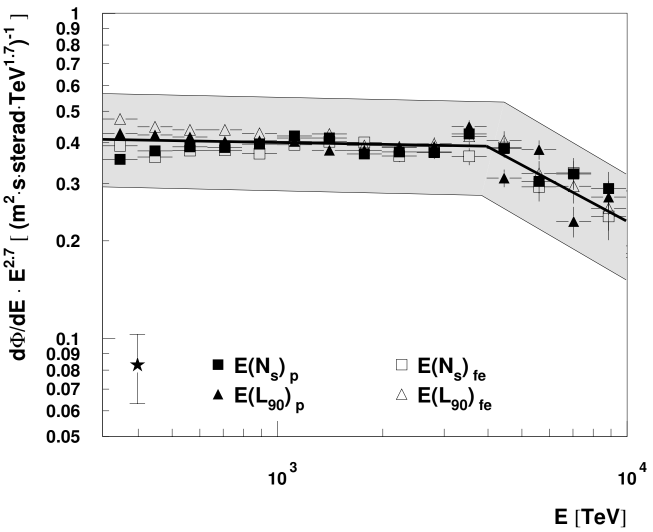


**Fig. 8.** The differential CR energy spectrum obtained with four energy reconstruction methods. Symbols are the same as in Fig. 6. The light shaded region represents systematical uncertainty. The "star" with vertical error bars shows the uncertainty of the HEGRA data originating from the 10% systematic uncertainty of the absolute energy scale that we estimate from the uncertainty in the determination of the absolute $N_s$ scale. The full line is the best fit as described in the text.

The spectral index for the spectrum below the knee is consistent with direct measurements at lower energies (Wiebel-Sooth et al. 1998) and a recent Cherenkov-light based determination of the spectral index in the TeV range (Aharonian et al. 1999); there is therefore no evidence for any change in spectral index from the TeV range right up to the knee.

### 6.3. Composition of CR

The fraction of light nuclei as a function of reconstructed energy - obtained from the fits to the measured penetration-depth distributions (see Sect. 5.2)- is presented in Fig. 10. At energies below the knee the composition is mixed and consistent with direct measurements around 100 TeV, namely $(p+\alpha)$/all = 0.54 ± 0.08 (Watson 1997). The data points seem to indicate a gradual enrichment of heavy elements above about 1 PeV though the error bars are large (remember that there are only six *independent* data points). We will discuss in Sect. 7 how reliable the qualitative conclusion of a gradual enrichment in heavy elements is within our systematic errors. The data rule out a predominantly light composition at all energies and does not give evidence for a drastic change of composition at the knee.

### 6.4. Elongation rate

Fig. 11 shows the corrected mean shower maximum depth as a function of energy. A least-squares fit to the $X_{\max}$ values as a function of energy, using only the statistical errors,

$$X_{\max} = \mathrm{ER} \times \log_{10}(\mathrm{E}) + \mathrm{ERB} \tag{6}$$

yields an elongation rate ER=78.3 ± 1.0 (stat) ± 6.2 (syst) g/cm$^2$ and mean depth parameter ERB=243.1 ± 2.6 (stat) ± 15.7 (syst) g/cm$^2$. The specified mean values and statistical errors are the mean of fit values with the four energy-reconstruction methods. The systematic error is estimated as the standard deviation of the mean values inferred with the four energy-reconstruction methods. The systematic error introduced by the systematic uncertainty in *slope* is smaller (about 3 and 14 g/cm$^2$ for ER and ERB respectively). The reduced $\chi^2$ values of the fit to relation (6) (4 d.o.f.) are very large (6.6,9.2,17.2,23.5) for energy-reconstruction methods 1–4, i.e the systematic errors dominate over the rather small statistical errors for the mean $X_{\max}$. Therefore the specified estimates of the statistical errors obtained with the procedure explained in Sect. 5.4 have to be treated with caution. The data point at the highest energy lies about 20 g/cm$^2$ higher in the atmosphere than expected for a constant elongation rate.

These results are not in contradiction with previous measurements in this energy range (Wdowczyk 1994; Turver 1992). This elongation rate, and also the absolute $X_{\max}$, is consistent with data at higher energies, obtained mainly by the Yakutsk and Fly's Eye collaboration (Watson 1997). A constant elongation rate of ≈ 73 g/cm$^2$ from 300 TeV up to $10^7$ TeV (dotted fit line in the summary diagram 10 in Watson 1997) is an intriguing hypothesis which is not in contradiction with our data.

### 6.5. Fluctuation of shower penetration depth

The RMS of the penetration depth distributions - calculated in reconstructed-energy bins, i.e. biased in favour of the light component of CR especially at low energies - is shown in Table 3. It does not show any obvious trend towards a heavy composition. Therefore the fact that the composition at the highest energy seems to be heavy with all energy reconstruction methods (Fig. 10) is mainly determined by the fact that the $X_{\max}$ in the highest energy bin lies about 20 g/cm$^2$ below a constant elongation rate.

## 7. Further studies of systematic uncertainties; analysis methods independent of absolute $X_{\max}$

The trend for an enrichment in heavy elements above the knee - which Fig. 10 suggest - is not significant within our errors. In this Sect. we elucidate this fact further, and explore what it would take to detect significantly a modest trend for an enrichment in heavy elements - as expected e.g. in a diffusion model of the knee (see Introduction) - with the present techniques. The agreement between the $X_{\max}$ distribution shape at low energies - predicted assuming a composition at low energies which is not very different from the one obtained by direct experiments - and the data (see Fig. 9) is satisfactory. This is an argument in favour of a correct MC simulation.

To explore the effect of our systematic error in *slope* (Sect. 5.4) Fig. 12 shows the results derived with an initial assumption of *slope* changed by 5% from its preferred value for energy-reconstruction method 3 and 4. It becomes clear that not

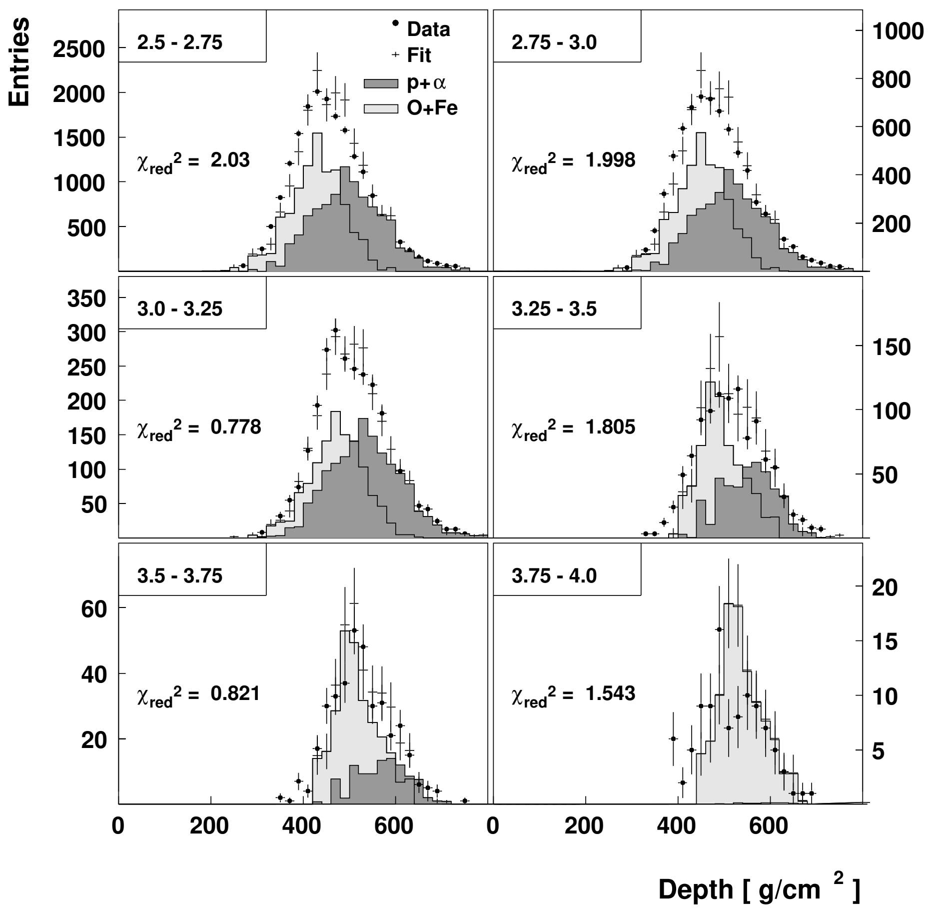


**Fig. 9.** The fit of MC expectations for light and heavier nuclei to the measured shower maximum depth distribution in the analysed reconstructed-energy intervals for method 3. The numbers in the upper left corner are the logarithms to the base of ten of the energy-bin boundaries in TeV. The full dots mark the experimental data with statistical errors, the crosses with error bars are the fitted MC distribution (where the errors correspond to the MC statistics). The two components fitted to the data are shown as dark shaded (large penetrations depths, light nuclei) and light shaded (heavy nuclei) histograms. Details of the procedure are described in the text.

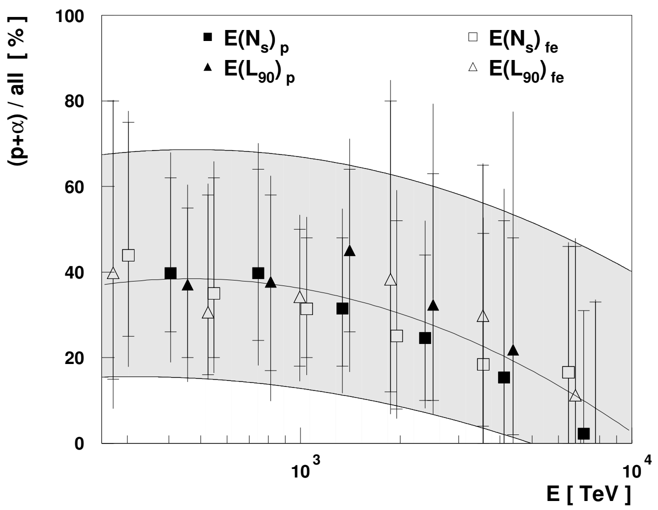


**Fig. 10.** The corrected fraction of light nuclei determined with four different energy reconstruction methods (see text for details). Each data point is plotted at the true mean energy of the events used to infer the mean $X_{\max}$. The error bars are statistical and systematic error added in quadrature (up to the tick-mark: only statistical error). The statistical errors are correlated due to the use of an identical Monte-Carlo sample in the first and last three energy intervals. The shaded band shows the allowed region between a polynomial fit to the upper and lower ends of the error bars.

only the mean but even the overall apparent "trend" may change, e.g. for method 3 with *slope* increased by 5% the composition appears to become *lighter* from the knee up to the penultimate bin. It should be stressed that none of the discussed "trends" is significant within our statistical errors.

The deviation of the penetration depth at the highest energy point from a constant elongation rate discussed in Sect. 6.5 is of the order of disagreements between different Monte Carlo codes at this energy(Heck et al. 1998). Therefore the possibility remains open that this deviation is due to a change in cascade characteristics not reliably modelled by the Monte Carlo, rather than to an enrichment in heavy elements. As it is also quite similar in size to our systematic error in slope, an origin in the HEGRA experiment for this deviation is also difficult to rule out.

Previous conference publications (Plaga et al. 1995; Cortina et al. 1997b; Cortina et al. 1998) are superseded by the present results - differences are mainly due to a more sophisticated amplifier calibration and the simpler energy reconstruction for the present analysis. In the last two of these publications, we tried to lessen the dependence of our composition result on the correct absolute $X_{\max}$ values by allowing a free "shift parameter"; the fit to the $X_{\max}$ was then performed with two free parameters: the ratio of light to all nuclei and an overall shift in penetration depth of all

**Table 3.** The RMS of the penetration depth distributions [g/cm$^2$] as a function of reconstructed energy (given in the same units as in Table 1) in the data and spectral Monte-Carlo sample. Given is the value inferred for the energy bins as defined with energy-reconstruction method 3, i.e. the specified values contain an A dependent bias. The first error is statistical and the second systematic (due to the systematic error in slope). For the numbers from Monte-Carlo simulations only a statistical error is given. "Mixed composition" represents the expectation for our best-fit chemical composition. Based on numerical experiments the statistical error was taken as the inferred value divided by $\sqrt{\text{number of events in bin}}$ rather than half of that, as would be correct for Gaussians, due to the non-Gaussian tails of the distribution. The comparison between experimental data and Monte Carlo simulations shows no trend towards a heavy composition at the higher energies.

| Rec. energy | Data | MC:mixed comp. | MC:p | MC:Fe |
|---|---|---|---|---|
| 2.5–2.75 (ca. 0.32–0.56 PeV) | $84 \pm 0.6 \pm 1.8$ | $77 \pm 2$ | $83 \pm 4$ | $50 \pm 3$ |
| 2.75–3. (ca. 0.56–1 PeV) | $80 \pm 0.9 \pm 1.4$ | | | |
| 3.0 - 3.25 (ca. 1–1.79 PeV) | $80 \pm 2 \pm 1.0$ | | | |
| 3.25–3.5 (ca. 1.79 -3.16 PeV) | $73 \pm 2 \pm 1.1$ | | | |
| 3.5–3.75 (ca. 3.16–5.62 PeV) | $67 \pm 3 \pm 1.5$ | $45 \pm 5$ | $73 \pm 17$ | $48 \pm 11$ |
| 3.75–4. (ca. 5.62–10 PeV) | $67 \pm 7 \pm 0.9$ | | | |

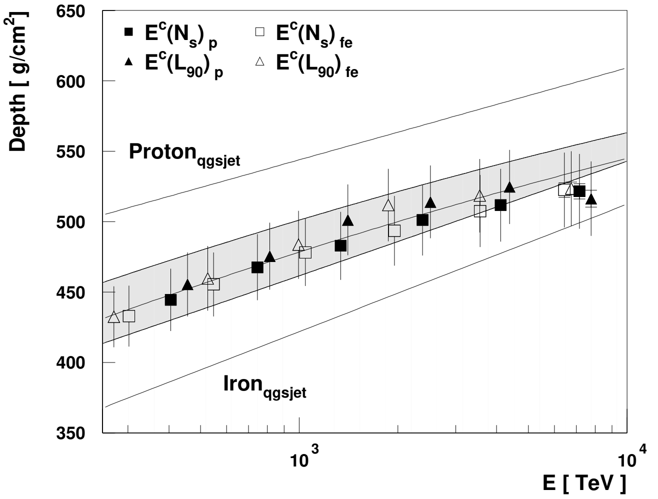


**Fig. 11.** The mean shower maximum depth as a function of energy using QGSJET simulations to model the EAS development. To obtain an unbiased elongation plot each data point is plotted at the true mean energy of the events used to infer the mean $X_{\max}$. The shaded region indicates the region expected from our best fit composition within its total error. Errors are statistical and systematical errors added in quadrature, up to the tick mark only statistical. Up to the highest energies the systematical error dominates.

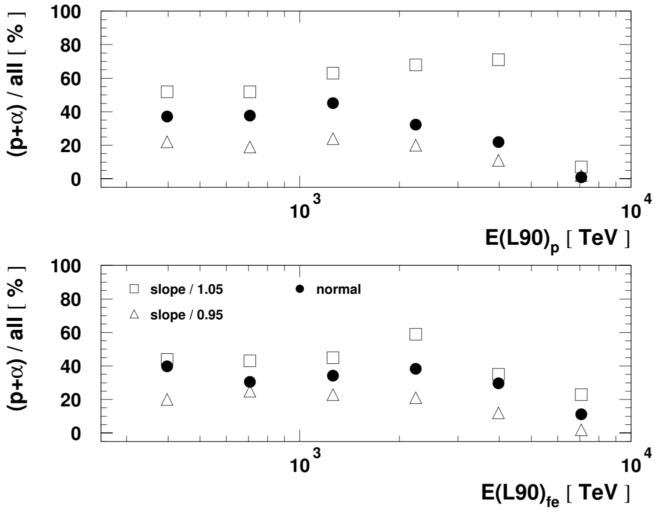


**Fig. 12.** The inferred chemical composition using energy-reconstruction method 3 (upper panel) and 4 (lower panel). The dots are the values as discussed before, the squares (triangles) are the results obtained when the *slope* is increased (decreased) by 5 % (the systematic error on this variable). The general "trend" (composition gets heavier/lighter) may change within this systematics.

MC distributions. In this way the result is mainly determined by the *shape* of the $X_{\max}$ distributions (in first order its width, i.e. RMS value). This width depends only weakly on a systematic uncertainty in the determination of *slope*, relative to the expected difference of a purely light or heavy composition.

Fig. 13 displays the result of such an attempt in a two dimensional plot showing the reduced $\chi^2$ for various "fraction of light nuclei" - "shift parameter" combinations for the data lowest and highest in energy. The shift is varied in an interval $\pm$ 30 g/cm$^2$, estimated from the likely systematic uncertainty of our detector and the Monte Carlo code. While in the low energy bin small (p+$\alpha$)/all ratios lead to unsatisfactory $\chi^2$ values for all shift values, in the highest energy bin - well above the knee - practically all fractions give acceptable $\chi^2$ values for appropriate shifts as seen in Fig. 13. The reason for this behaviour is that - given the small number of events in the high-energy bin - the $X_{\max}$ distribution can be fitted both with the relatively broad predominantly light composition shifted to larger depths in the atmosphere and a mixed heavy/ light composition (where the difference in mean penetration depth of the heavy and light component contributes to the total width) shifted to small penetration depth. We have to conclude that it is not reliably possible to determine the composition based mainly on the width of the $X_{\max}$ distribution. We found in numerical experiments that with this method, and assuming a Monte-Carlo simulation describing the experimental data well, together with a statistics increased by about a factor of 100 (which is difficult but not impossible to reach in future experiments) it will just be possible to reach the desired precision of 10% mentioned in the introduction on a $2\sigma$ level beyond the knee.

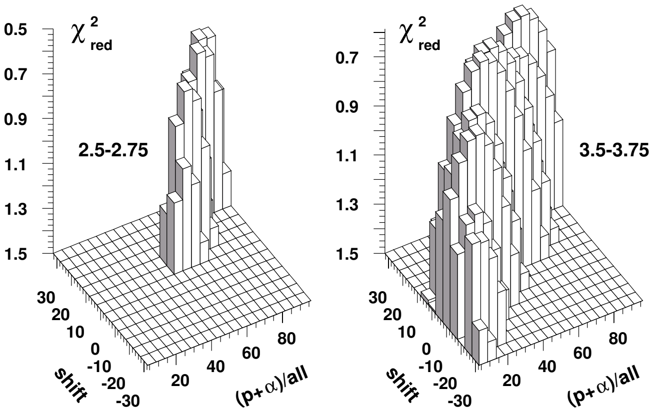


**Fig. 13.** The reduced $\chi^2$ values (z-axis) of a description of the measured penetration- depth distribution with the spectral Monte Carlo data as a function of "fraction of light nuclei" (y-axis) and overall shift in depth (x-axis). Only acceptable $\chi^2$ values smaller than 1.5 are displayed. The energy was reconstructed assuming protons and using the the Cherenkov light density (method 3). The left panel is for the first energy bin ($\log_{10}$E[TeV]=2.5–2.75, 19000 data events, 1460 Monte-Carlo events) the right panel for the penultimate one ($\log_{10}$E[TeV]=3.5–3.75, 369 data events, 98 Monte-Carlo events). In the high-energy bin practically all chemical compositions are allowed for certain "shifts".

## 8. Conclusion

The results of this paper demonstrate that our data seem to be well described by the QGSJET hadron generator within the CORSIKA program: The energy spectra derived with different air-shower observables and assumptions about the chemical composition of CR differ only within the estimated systematic errors. This is an argument in favour of the contention that the "knee" is a feature in the primary flux of cosmic rays, rather than some new effect in the interaction of cosmic rays at very high energies. Such a new effect would probably lead to inconsistencies in the data analysed by a generator that does not take them into account.

Up to the knee we find a mixed composition and an energy-spectrum power law index consistent with the results of direct experiments at energies around 100 TeV. The data favour a gradual enrichment in heavy elements at energies above the knee but the systematic errors of our experiment do not allow to rule out a constant composition. An abrupt change of composition or a substantial enrichment in light elements at the knee is ruled out. We find an elongation rate of about 78 g/cm$^2$ and a mean penetration depth consistent with other experimental data on CR with energies higher than studied here (Watson 1997).

*Acknowledgements.* We thank the Instituto de Astrofisica de Canarias (IAC) and the ORM observatory for support and excellent working conditions. We are grateful to the authors of CORSIKA and to the KASCADE collaboration for many stimulating discussions. The experiment HEGRA is supported by the German BMBF and DFG and the Spanish CICYT.

## References

Aharonian F., Akhperjanian A.G., Barrio J.A., et al. (HEGRA coll.), 1999, Phys.Rev. D59, 092003

Allen G.E., Keohane J.W., Gotthelf E.V., et al., 1997, ApJ 487, L97

Bernlöhr K., 1999, astro-ph/9908093, Astropart. Phys. in press

Biermann P.L., Gaisser T.K., Stanev T., 1995, Phys.Rev. D51, 3450

Buckley J.H., Akerlof C.W., Carter-Lewis D.A., et al. (WHIPPLE coll.), 1998, A&A 329, 639

Bykov A.M., Toptygin I.N., 1997, In: Potgieter M.S. et al. (eds.) Proc. 25$^{th}$ ICRC Durban 1997 vol.4 p.365.

Cortina J., Horns D., Kornmayer H., et al. (HEGRA coll.), 1997a, In: Potgieter M.S. et al.(eds.) Proc. 25$^{th}$ ICRC Durban 1997 vol.4 p.69.

Cortina J., Arqueros F., Lorenz E., 1997b, J.Phys.G 23, 1733

Cortina J., 1998, PhD thesis, University of Madrid

Cortina J., Horns D., Kornmayer H., et al. (HEGRA coll.), 1998, In: Medina J. (ed.) Proc 16$^{th}$ ECRS Alcala de Henares 1998 p.531

Gaisser T.K., 1997, Nucl.Phys.B (Proc. Suppl.) 52B, 10

Greisen K., 1956, Prog. Cosmic Ray Physics 3, 1

Haustein V., 1996, PhD Thesis, University of Hamburg

Heck D., Knapp J., Capdevielle J.N., Schatz G., Thouw T., 1998, FZKA report 6019

Heß M., 1997, In: In: Potgieter M.S. et al.(eds.) Proc. 25$^{th}$ ICRC, Durban vol.3 p.229

Horns D., 1997, Diploma Thesis, HH-HEGRA/97-02, University of Hamburg

Jokipii J.R., Morfill G., 1987, ApJ 313, 842

Kalmykov N.N., Ostapchenko S.S., Pavlov A.I., 1997, Nucl. Phys. B (Proc.Suppl.) 52B, 17

Karle A., Merck M., Plaga R., et al., 1995, Astropart.Phys. 3, 321

Knapp J., Heck D., 1993, KFK report 5196B

Knapp J., Heck D., Schatz G., 1996, FZKA report 5828

Konopelko A., Hemberger M., Aharonian F., et al. (HEGRA coll.), 1999, Astropart.Phys. 10,275

Kornmayer H.,1999, PhD thesis, University of Munich

Koyama K., Petre R., Gotthelf E., et al.,1995, Nat 378, 255

Koyama K., Kinugasa K., Matsuzaki, K., et al., 1997 PASJ 49, 7

Krawczynski H., Prahl J., Arqueros, F., et al. (HEGRA coll.), 1996, Nucl.Inst.Meth A 383, 431

Lindner A., 1997, In: Potgieter M.S. et al. (eds.) Proc. 25$^{th}$ ICRC, Durban, vol.5 p.113

Lindner A., 1998a, Astropart.Phys. 8, 235

Lindner A., 1998b, HEGRA coll. internal note "On the Energy Spectrum and Composition: a new Analysis assuming primary Protons".

Martinez S., Arqueros F., Fonseca V., 1995, Nucl.Inst.Meth. A 357, 567

Patterson J.R., Hillas A.M.J., 1983, Phys.G 9, 1433

Peters B., 1961, Nuovo Cim. 22, 800

Plaga R., Karle A., Arqueros F., et al. (HEGRA coll.), 1995, In: Iucci N. (ed) Proc. 24$^{th}$ ICRC Rome 1995 vol.2 p.693

Prosch C., Feigl E., Plaga R., et al. (HEGRA coll.), 1996, A&A, 314, 275

Protheroe, R., Szabo, A.P., 1992, Phys.Rev.Lett. 69, 2885

Ptuskin V.S., Rogovaya S.I., Zirakashvili V.N., et al.,1993, A&A 268, 726

Rhode W., Becker K.H., Daum K., et al., 1996, Nucl.Inst.Meth. A378, 399

Stanev T., Biermann P.L., Gaisser T.K., 1993, A&A 274, 902

Tanimori T., Hayami Y., Kamei S., et al., 1998, ApJ 497, L25

Turver K.E., 1992, Nucl.Phys.B (Proc. Suppl.) 28B, 16

Völk H.J., 1997, In: de Jager O.C. (ed.), Proc. Krüger Park Work. on TeV Gamma Ray Astrophysics, p.87, astro-ph/9711204

Watson A.A., 1997, In:M.S.Potgieter et al.(eds.) Proc. 25$^{th}$ ICRC (Durban), Invited and Rapp. Talks, vol.8 p.257

Wdowczyk J., 1994, Phys. G 20, 1001

Wiebel-Sooth B., 1998, PhD thesis University of Wuppertal, WUB-DIS 98-9

Wiebel-Sooth B., Biermann P.L., Meyer H., 1998, A&A 330, 389